Driver Transport System", CEBAF-TN-96-026, 6 June 1996, or visit The FODOmat, at

http://www.cebaf.gov/~douglas/

[12] See Reference 9.

[13] R. Li, J. Bisognano, and C. Bohn, work in progress.

[14] R. Li, work in progress. The observations in this section are based on her work. Any errors, however, are my responsibility.

[15] See Reference 9.

[16] *ibid*.

[17] *ibid*., Reference 11.

[18] TLIE studies by R. Li, *op. cit*.

[19] See various CEBAF Technical Notes and Reports by R. Li, H. Liu, L. Merminga and B. Yunn documenting their work on these topics.

http://www.cebaf.gov/~douglas/

VI. Acknowledgments

I would like to thank Leigh Harwood, Andrew Hutton, Bob Legg, and all members of the CEBAF FEL Group for useful discussions while generating this design. Many of the concepts employed herein originated with them. I would like to thank Christoph Leemann for several discussions over previous months, which have strongly influenced both the philosophy and direction of this study. In addition, I would like to thank Dr. Jay Flanz for extremely useful guidance on both the concept and the execution of this design and its details, and the analysis of its performance. His input and ideas have been of tremendous value. Finally, I would like to thank Fred Dylla for his support and encouragement during this work.

VIII. References

[1] G. Neil, private communication.

[2] *ibid*.

[3] H. Liu, private communication.

[4] *ibid*.

[5] J.B. Flanz, S. Kowalski, and C.P. Sargent, “An Isochronous Beam Recirculation Magnet System”, I.E.E.E. Transactions on Nuclear Science, Vol. NS-28, No. 3, June 1981; J.B. Flanz and C.P. Sargent, “Operation of an Isochronous Beam Recirculation System”, Nuclear Instruments and Methods in Physics Research, A241 (1985), pp. 324-333, North Holland, Amsterdam; J.B. Flanz, and C.P. Sargent, “Tests With An Isochronous Recirculation System”, I.E.E.E. Transactions on Nuclear Science, Vol. NS-32, No. 5, October 1985.

[6] G. Neil, *op.cit*.

[7] See, for example, Section 4.3 of “Free-Electron Lasers for Industry”, Volume 2, UV Demo Conceptual Design, Laser Processing Consortium, January 1996; this is the UV Demo conceptual design report.

[8] J. Flanz *et.al*, *op. cit*.

[9] D. Douglas, “Error Estimates of the IR FEL Transport System”, CEBAF-TN-96-035, 15 July 1996.

[10] J. Flanz, private communication.

[11] See, for example, D. Douglas, “Engineering Design Specifications For IR FEL

Preliminary analytic error studies have been completed and engineering specifications made [17]. Ongoing work will evaluate higher order aberration effects [18] and simulate numerically sensitivities to alignment, powering, and magnetic field quality errors.

Our primary remaining technical concerns are as follows:

- Sensitivity to injection errors (T_{ij6} aberrations)
- Short magnets with large apertures - will be essentially 3-dimensional, hard to model, need to compensate
- lattice provides limited capacity to compensate errors
  - adjustable momentum compaction/dispersion
  - adjustable match to/from wiggler,
  - very limited phase advance control (BBU thresholds)
  - very limited control of chromatic aberrations

In this design, many optimizations and operational functions are performed using hardware (for example, through the choice of bend radius, pole face rotations, or element spacings). This is a good solution for a production machine and will be great if the machine works well, but fall-back positions are few and weak. These issues will be addressed through the studies that are in progress and during commissioning.

Beam dynamics analysis for this machine (BBU, CSR, impedance, RF stability, space charge effects) has been underway for some time and indicates that the design should operate successfully [19]. BBU and other impedance effects should not be a problem; studies of CSR and RF stability are well underway. Space charge effects have been simulated from injector to wiggler and are anticipated to be a problem; further simulations of the full acceleration/energy recovery cycle are still to be performed. Studies of various operation scenarios, such as those which follow, will be ongoing.

Operational Scenarios:

- orbit correction algorithms
- beam properties measurement/matching/correction
- injection error tolerances
- rf cavity skew quad compensation, head-tail emittance dilution, *etc.*
- energy compression to reduce 25% momentum spread at end of energy recovery; M_{56}, T_{566} choices, transport system behavior for nonzero values of T_{566}
- CSR optimization retuning (backleg phase advance)
- energy variations (28 MeV for 6 micron light; injection chicane energy acceptance, *etc.*)

Updates to the driver design and status reports on the above topics may be found on the World Wide Web at

Path Length/Momentum Compaction Tunability:
The optical behavior of the return arc for different path-length and momentum compaction settings has been scanned simultaneously over ranges of ±10 cm in path length and ±0.25 m in M_{56}. At each desired path length (set by steering through the π-bend, as discussed above), the arc dispersion and M_{56} are set by use of trim quads; and the sextupole correction adjusted to hold T_{166}, T_{266}, and T_{566} to zero.

Beam properties are then studied using the DIMAD tools employed above. Principle Table 1 requirements are met over this region of the parameter space. Minor exceptions do arise. For example, peak off-momentum beam envelopes pop up to ~30 m in isolated locations; phase spaces do however remain regular and well-controlled, so these features are not anticipated to be problematic. M_{16}, M_{26}, and M_{56} vary by a few centimeters over the full pathlength range, and remnant orbits of ~1 mm are generated. These minor perturbations can be readily accommodated operationally using the available correction systems.

V. Design Status/Summary

We have described a detailed design of the “downstream wiggler option” for the driver accelerator of the TJNAF 1 kW IR FEL Demo. This design has been “frozen” since 16 May 1996, and is detailed in the following DIMAD input/output files.

~douglas/../../../../prinzipal/usr/users/optics/IRFEL_optics/irapr96/baseline/irfelbaseline05161996

~douglas/../../../../prinzipal/usr/users/optics/IRFEL_optics/irapr96/baseline/irfelbaseline05161996out

This design meets the machine requirements detailed above. Minor design updates (such as finalization of injection/reinjection/energy recovery dump chicanes to 10 MeV/42 MeV kinetic energy ratios, design of dump beam lines, *etc.*) have been or will be placed in the following directory.

~douglas/../../../../prinzipal/usr/users/optics/IRFEL_optics/asbuilt

Individual optical solutions will be documented as needed. In this note, most studies used the optics developed in the following DIMAD input file, in which a 19 cm nominal momentum compaction from wiggler to linac is available and element-to-element phase advances are adjusted to optimize diagnostic and correction system performance.

~douglas/../../../../prinzipal/usr/users/optics/IRFEL_optics/problems/simulation/906test

Figure 13c: Phase space with injection error of y'=1 mrad.

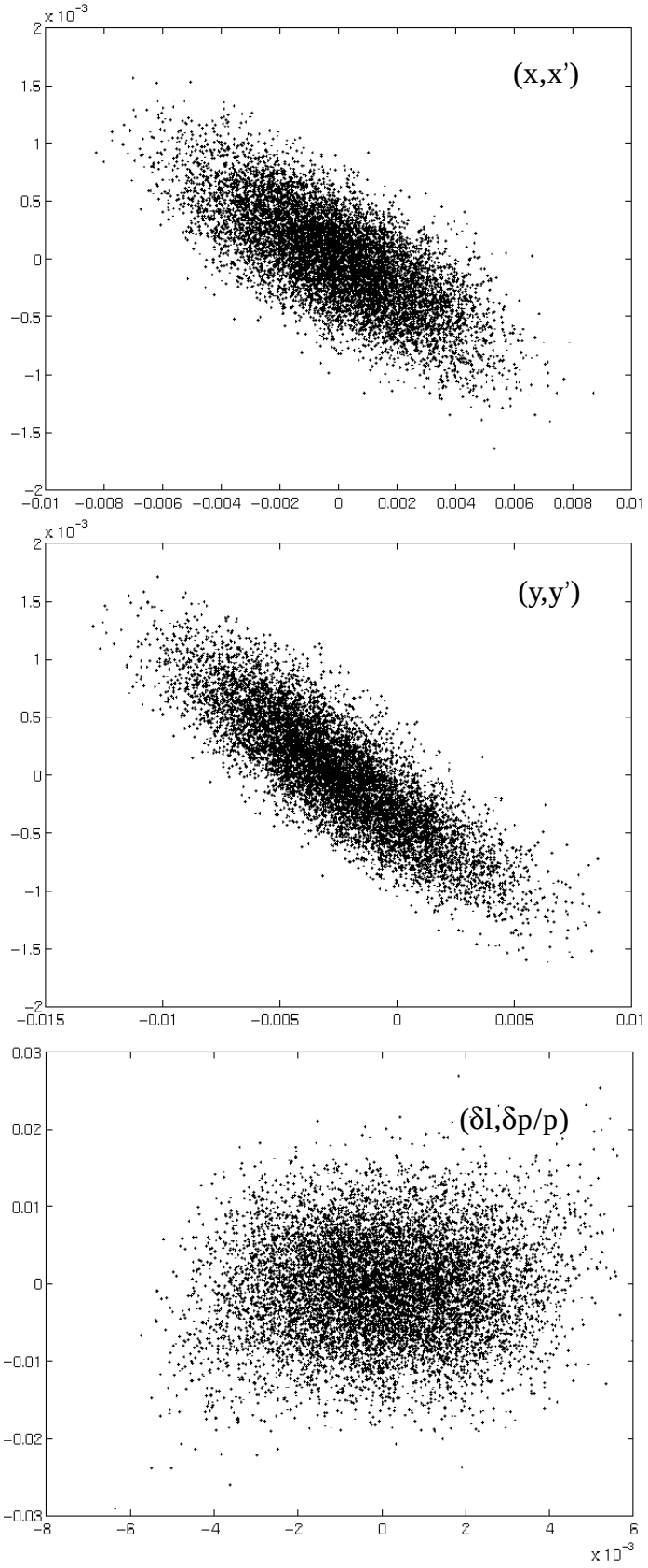

Figure 13b: Phase space with injection error of y=1 mm.

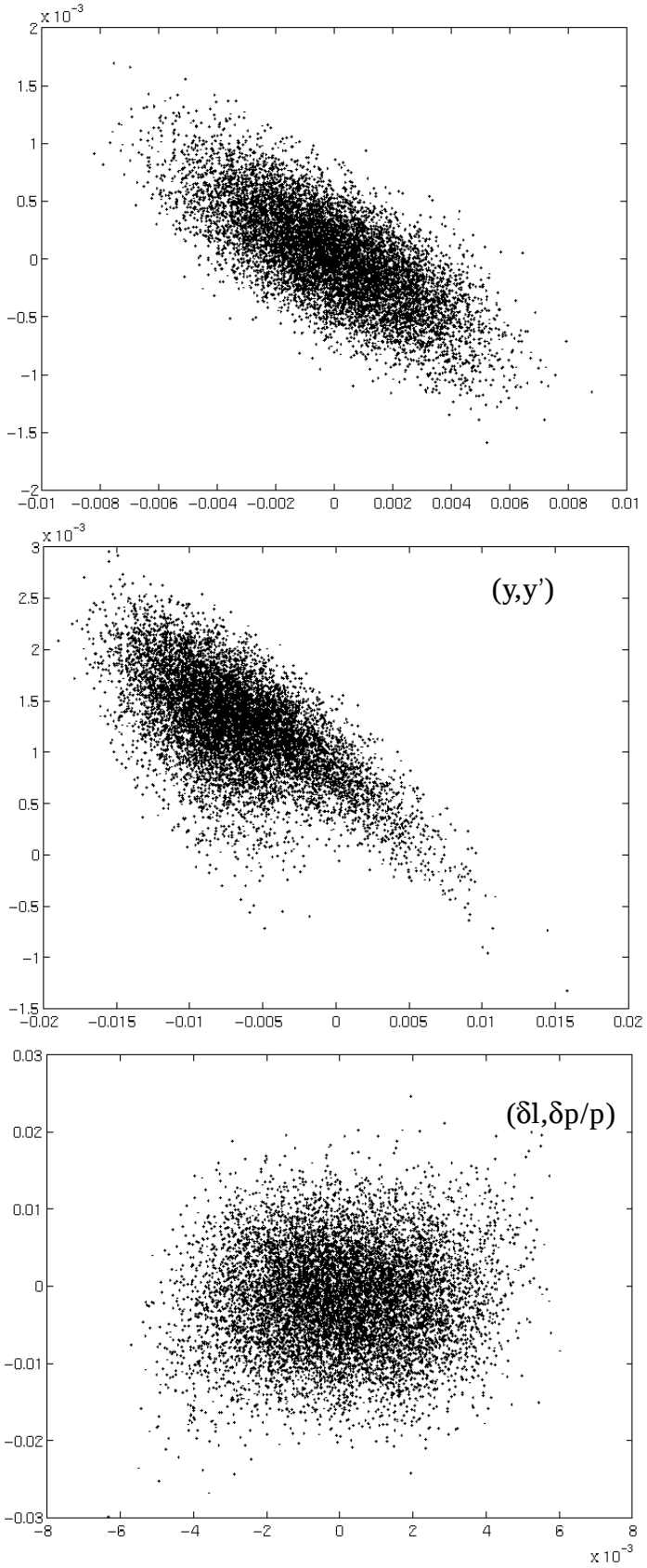

Figure 13a: Phase space at end of cryomodule after energy recovery

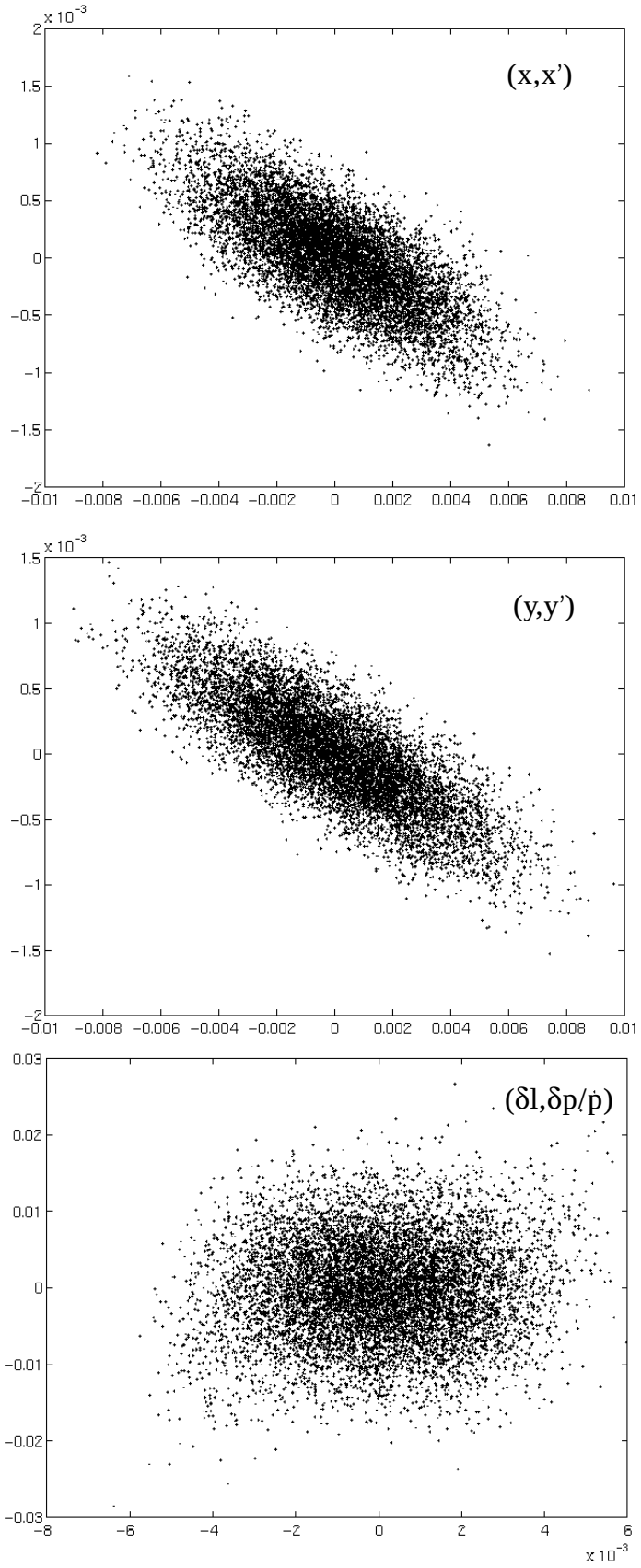

Initial Load, Misteered in y by 1 mm

```
 AVERAGES FOR X,XP,Y,YP,L,DELTA ARE
    .25066E-05    .98376E-05    .99992E-03    .72526E-05   -.27146E-06   -.12515E-03

 STDDEV FOR X,XP,Y,YP,L,DELTA ARE
    .27669E-03    .59282E-03    .28290E-03    .56777E-03    .29853E-03    .10169E-01

 THE FULL BEAM MATRIX IS :
    .2767E-03   .1782E-01  -.1740E-02  -.5012E-02   .1402E-01  -.2440E-02
                .5928E-03   .3019E-02  -.4483E-02  -.7269E-02  -.1312E-01
                            .2829E-03   .1122E-02   .8838E-02   .1031E-01
                                        .5678E-03   .1389E-01  -.1210E-01
                                                    .2985E-03  -.1313E-02
                                                               .1017E-01
```

Final Phase Space, Misteered in y by 1 mm

```
 AVERAGES FOR X,XP,Y,YP,L,DELTA ARE
   -.85694E-04    .29169E-04   -.65667E-02    .12583E-02    .47170E-04   -.15254E-02

 STDDEV FOR X,XP,Y,YP,L,DELTA ARE
    .23435E-02    .41966E-03    .43842E-02    .49344E-03    .19125E-02    .65714E-02

 THE FULL BEAM MATRIX IS :
    .2344E-02  -.7232E+00  -.1987E-01   .1049E-01  -.1974E-01  -.2122E-01
                .4197E-03   .1840E-01   .2414E-01  -.1147E-01   .6752E-02
                            .4384E-02  -.6471E+00  -.7213E+00  -.8791E-01
                                        .4934E-03   .1066E+00  -.6326E-01
                                                    .1913E-02   .5377E-01
                                                                .6571E-02
```

Initial Load, Misteered in y' by 1 mrad

```
 AVERAGES FOR X,XP,Y,YP,L,DELTA ARE
    .25066E-05    .98376E-05   -.83264E-07    .10073E-02   -.27146E-06   -.12515E-03

 STDDEV FOR X,XP,Y,YP,L,DELTA ARE
    .27669E-03    .59282E-03    .28290E-03    .56777E-03    .29853E-03    .10169E-01

 THE FULL BEAM MATRIX IS :
    .2767E-03   .1782E-01  -.1740E-02  -.5012E-02   .1402E-01  -.2440E-02
                .5928E-03   .3019E-02  -.4483E-02  -.7269E-02  -.1312E-01
                            .2829E-03   .1122E-02   .8838E-02   .1031E-01
                                        .5678E-03   .1389E-01  -.1210E-01
                                                    .2985E-03  -.1313E-02
                                                               .1017E-01
```

Final Phase Space, Misteered in y, by 1 mrad

```
 AVERAGES FOR X,XP,Y,YP,L,DELTA ARE
   -.54239E-04    .97661E-05   -.25399E-02    .18487E-04   -.20586E-05   -.47319E-03

 STDDEV FOR X,XP,Y,YP,L,DELTA ARE
    .23425E-02    .41874E-03    .31796E-02    .50394E-03    .19091E-02    .65491E-02

 THE FULL BEAM MATRIX IS :
    .2342E-02  -.7230E+00  -.2792E-01   .4793E-01  -.4350E-01  -.2820E-01
                .4187E-03   .4049E-01  -.4723E-01   .2533E-01   .2006E-01
                            .3180E-02  -.8475E+00   .4990E+00   .1315E+00
                                        .5039E-03  -.5899E+00  -.1305E+00
                                                    .1909E-02   .6587E-01
                                                                .6549E-02
```

Energy Recovery:

The energy recovery process has been simulated and appears viable from the perspective of beam transport. A 6σ gaussian load of 10000 particles was injected at the wiggler center with an rms geometric emittance of 0.16 mm-mrad, an rms bunch length of 1 psec (0.3 mm) and an rms momentum spread of 1%. These rays were traced through the system with DIMAD from wiggler to the extraction point using an energy-compression tuning (M_{56} of 0.19 m from wiggler to cryomodule). Figure 13 provides scatter-plots of the energy-recovered phase space. RMS values for all phase space dimensions before and after the transport (from a DIMAD "particle distribution analysis") agree with the prediction of linear transport to ~20% or better. For example, linear transport predicts an 0.27 mm rms vertical spot as follows.

$$\sigma_y = \sqrt{\beta_y \varepsilon} \sim \sqrt{11\ \text{m} \times 0.16 \times 10^{-6}\ \text{m-rad} \times (42\ \text{MeV} / 10\ \text{MeV})} \sim 0.27\ \text{mm}$$

Numerical simulation results, given in Table 3, also predict an rms vertical spot size of 0.27 mm. Figure 13 provides scatter-plots of the energy-recovered phase space. We have also simulated the effect of T_{ij6} aberrations coupling to injection errors. We confirmed that spot growth for 1 mm or 1 mrad injection errors are ~50% of the nominal spot size. As noted above, this is achieved through optimization of the lattice. The effect is operationally limited to negligible levels by FEL steering requirements.

Table 3: Results of DIMAD Simulation of Energy Recovery

Initial Load

```
 AVERAGES FOR X,XP,Y,YP,L,DELTA ARE
    .25066E-05    .98376E-05   -.83264E-07    .72526E-05   -.27146E-06   -.12515E-03

 STDDEV FOR X,XP,Y,YP,L,DELTA ARE
    .27669E-03    .59282E-03    .28290E-03    .56777E-03    .29853E-03    .10169E-01

 THE FULL BEAM MATRIX IS :
    .2767E-03   .1782E-01  -.1740E-02  -.5012E-02   .1402E-01  -.2440E-02
                .5928E-03   .3019E-02  -.4483E-02  -.7269E-02  -.1312E-01
                            .2829E-03   .1122E-02   .8838E-02   .1031E-01
                                        .5678E-03   .1389E-01  -.1210E-01
                                                    .2985E-03  -.1313E-02
                                                               .1017E-01
```

Final Phase Space

```
 AVERAGES FOR X,XP,Y,YP,L,DELTA ARE
   -.84211E-05    .64421E-05   -.41241E-04    .27171E-05   -.13464E-04   -.22522E-03

 STDDEV FOR X,XP,Y,YP,L,DELTA ARE
    .23411E-02    .41861E-03    .26983E-02    .40247E-03    .19101E-02    .65344E-02

 THE FULL BEAM MATRIX IS :
    .2341E-02  -.7230E+00  -.1010E-01   .2047E-02  -.3987E-01  -.2832E-01
               .4186E-03   .5686E-02   .1354E-02   .1958E-01   .1855E-01
                           .2698E-02  -.7969E+00   .4066E-02   .1794E-01
                                       .4025E-03   .3151E-02  -.1402E-01
                                                   .1910E-02   .6306E-01
                                                               .6534E-02
```

cal T_{ij6} numbers are of order 100 m/m-rad or 100 m/(rad^2), so injection orbit errors at 1 mm/1 mrad level generate spurious dispersions at the 10 cm level. This leads to off-momentum centroid motions (spot growth) of ~2-3 mm at 2.5% momentum offsets. Potentially, the final spot size can as much as double. Control of such aberrations is therefore important, and an understanding of their potential impact is needed.

The lattice *has* been optimized to reduce the aberration level; the design attempts to provide control through appropriate selection of beamline parameters (bend radii, angles, pole face rotations, *etc.*). The ~100 m/m-rad or 100 m/(rad^2) is the residual after optimization. A more precise bound on the potential impact may be obtained by noting that the spot size growth must be convoluted with the momentum distribution of the full bunch. When raytracing from wiggler to dump is performed with a gaussian bunch, the net effect is only ~50% growth in rms spot size at end of system (after energy recovery) when 1 mm or 1 mrad injection errors are imposed. This result is discussed in more detail in a following treatment of energy recovery, but is immediately seen as a significantly smaller effect than the estimated doubling in spot size described above.

The impact of such aberrations can also be limited by appropriate injection orbit control. The cited 1 mm/1 mrad injection errors at the wiggler are, in fact, intolerably large for FEL operation. A tighter injection orbit error tolerance (such as 0.1 mm/0.1 mrad) will provide adequate control of this effect and must in any event be imposed for FEL operation.

A second effect noted in the preliminary TLIE studies is that the rolloff of horizontal orbit with momentum is somewhat harder than that predicted by DIMAD (Figure 10a). DIMAD predicts x and x' at the ±3% momentum limits of ~200 μm and ~60-80 μrad, respectively. TLIE predicts similar x offsets, but larger x' offsets of ~150 μrad, suggesting a somewhat stronger rolloff of x'(δ) with δ. Though quantitatively different, the effect is qualitatively like that in DIMAD; this strong rolloff can be observed with DIMAD at slightly larger momentum offsets of 3.5 to 4%. In either case, the relative emittance growth is small - less than a factor of 2. In this context, it was determined that the central orbit variation with momentum is rather sensitively dependent on sextupole setting. A 3% variation in the recirculator sextupoles can eliminate the 150 μrad x' variation at 3% momentum offset. This is not surprising; arguing as in the FEL error analysis study [15], one notes only that a particle with 3% momentum offset will be at a displacement of ~6 cm at the sextupole (where the dispersion is of order 2 m) and will experience a kick of ~2 mrad relative to the central orbit. A 3% variation in sextupole field leads to a variation of this kick of order 60 μrad. Assuming an rms M_{22} of ~1/2 from the eight sextupoles to the end of the arc, this would generate an x' variation of 8 x 1/2 x 60 μrad, or 240 μrad. This is the order of magnitude of the observed effect. The 2.5×10^{-3} powering tolerance on the sextupoles [16] will avoid problems with this effect by reducing it to a negligible 10-15 μrad level.

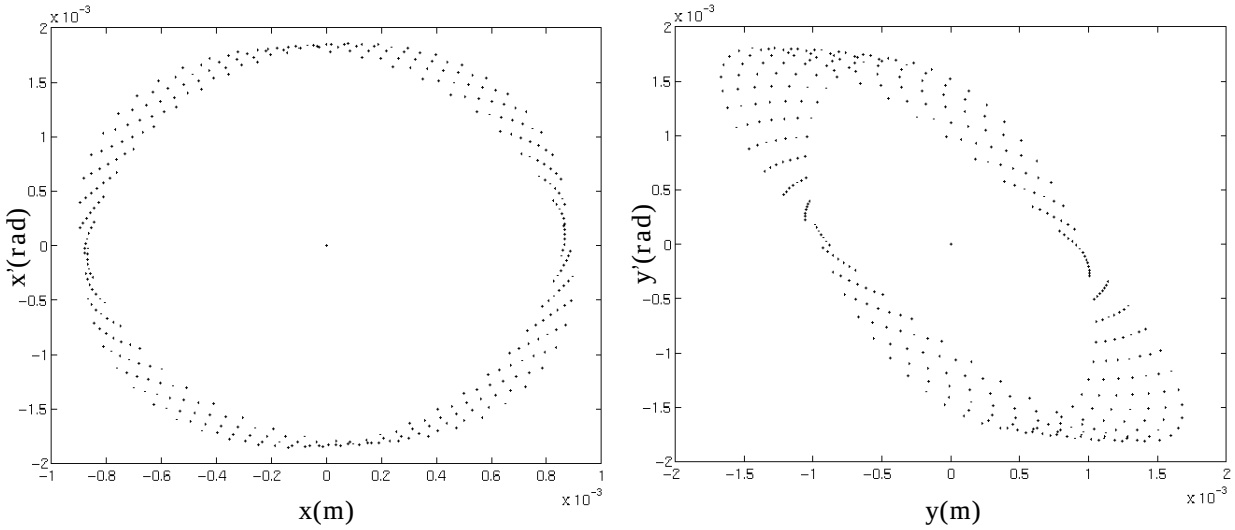

Figure 12a: Image at wiggler of matched ellipses launched from cryomodule at each of seven momentum offsets across a momentum range of ±3%.

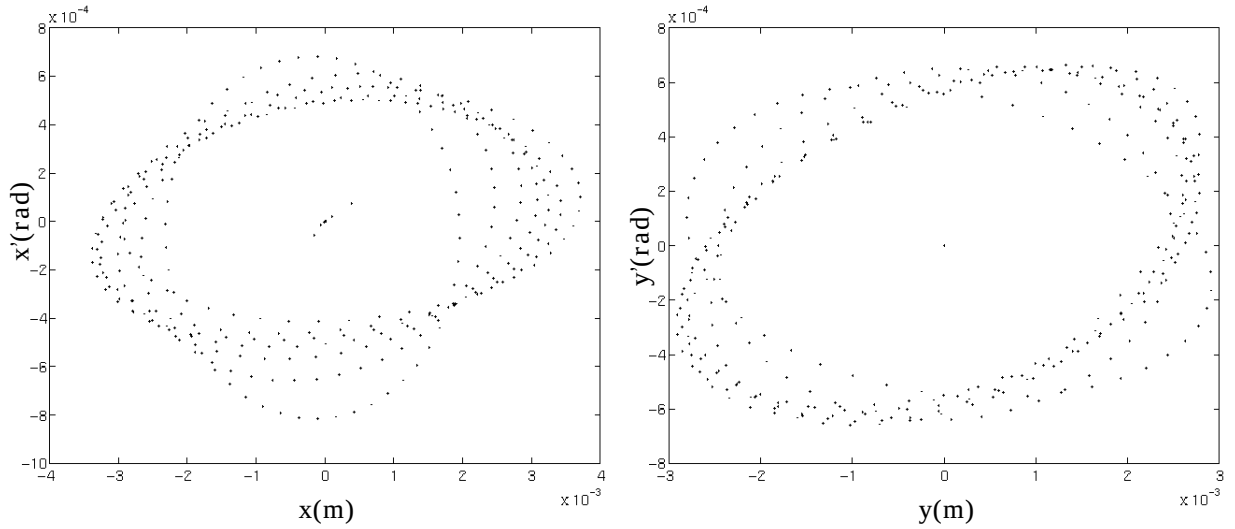

Figure 12b: Image at reinjection point of matched ellipses launched from wiggler at each of seven momentum offsets across a momentum range of ±3%.

High Order Nonlinear Analysis:

TLIE analysis by Li has commenced [14]; preliminary results confirm qualitatively the performance described above. Two observations made as a part of this analysis are of note. Firstly, T_{126}-like aberrations inherent to lattices such as these can in principle cause sensitivity to injection condition, leading to spot spreads of as much as several millimeters over the full momentum range during energy recovery. Typi-

Geometric Aberrations:

Amplitude dependences of the transport have been investigated using the “line geometric aberrations” operation in DIMAD. In this study, initially “matched” phase ellipses at ten times the nominal geometric emittance of 0.16 mm-mrad are tracked at momentum offsets from -3% to +3% in 1% steps either from cryomodule to wiggler or from wiggler to cryomodule. In either case, tracking results are acceptable. Both “linac to wiggler” and “wiggler to linac” simulations show good beam behavior over the examined region phase space, with output phase ellipses exhibiting only modest distortion.

In particular, the phase space distortion $\Delta\varepsilon/\varepsilon$ over the full momentum range and at ten times the nominal emittance is, in either plane, less than 0.02 from linac to wiggler and less than 0.25 from wiggler to linac. This is better than the specification in Table 1. The supporting data are presented in Figure 11. Figure 12 shows the image phase spaces at wiggler and reinjection point of matched ellipses launched, respectively, at cryomodule and wiggler, at each of seven momentum offsets through the full momentum range of ±3%. The ellipses are without significant distortion, are well matched at the wiggler, and well confined at the reinjection point. The transport therefore is expected to experience little performance degradation from geometric aberrations.

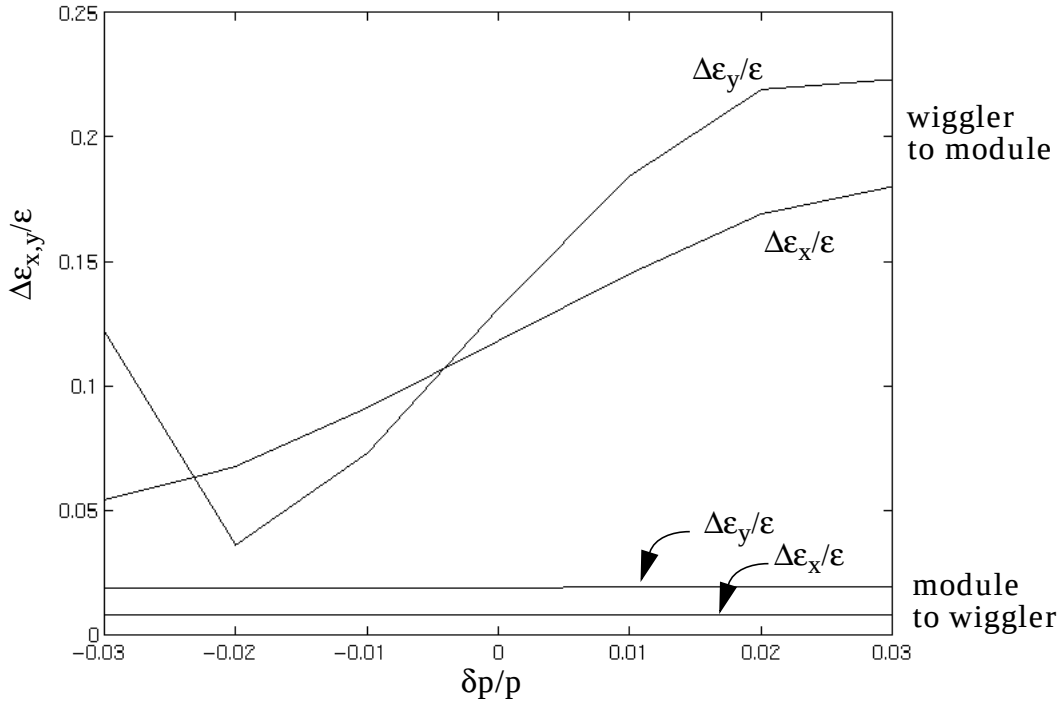

Figure 11: Phase space distortion $\Delta\varepsilon/\varepsilon$ over the full momentum range at ten times the nominal emittance from linac to wiggler and wiggler to linac.

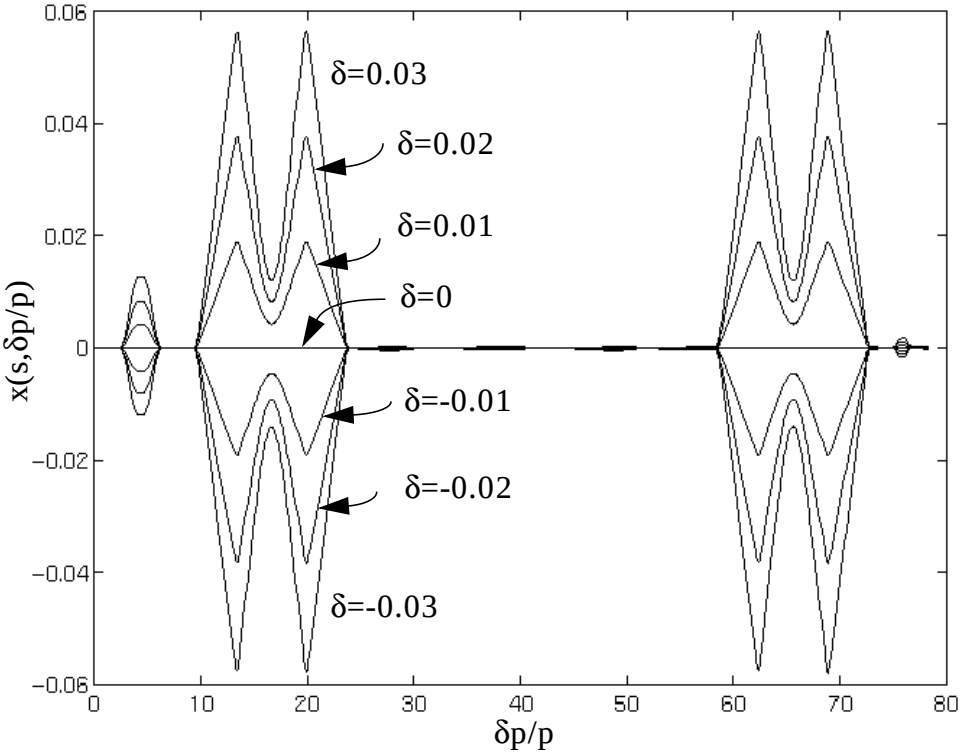

Figure 10a: - x vs. s at several δp/p from wiggler to reinjection point.

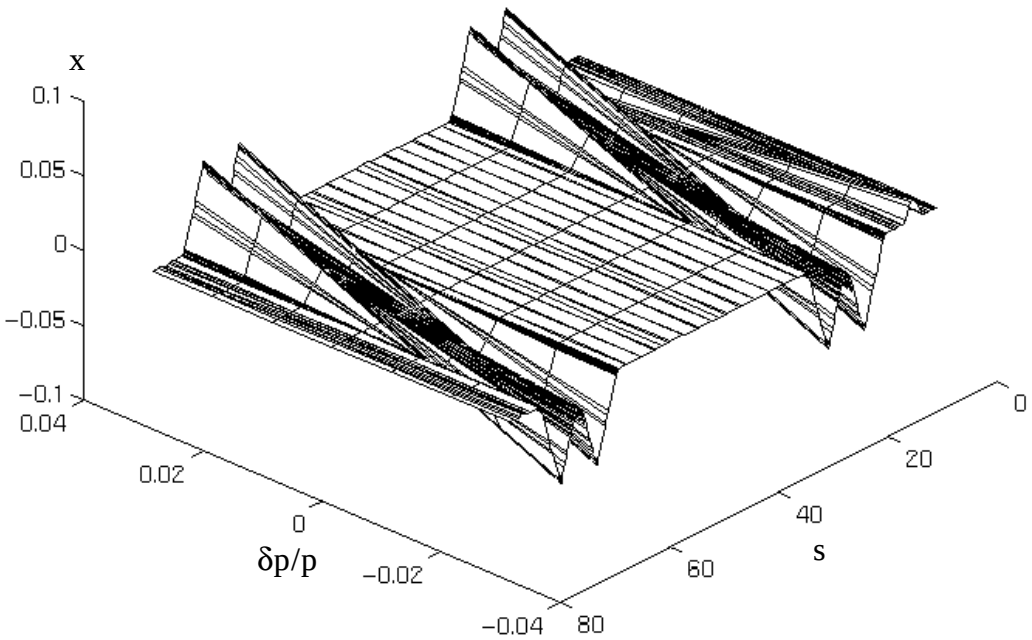

Figure 10b: - Alternate presentation of x(s, δp/p) from wiggler to reinjection point.

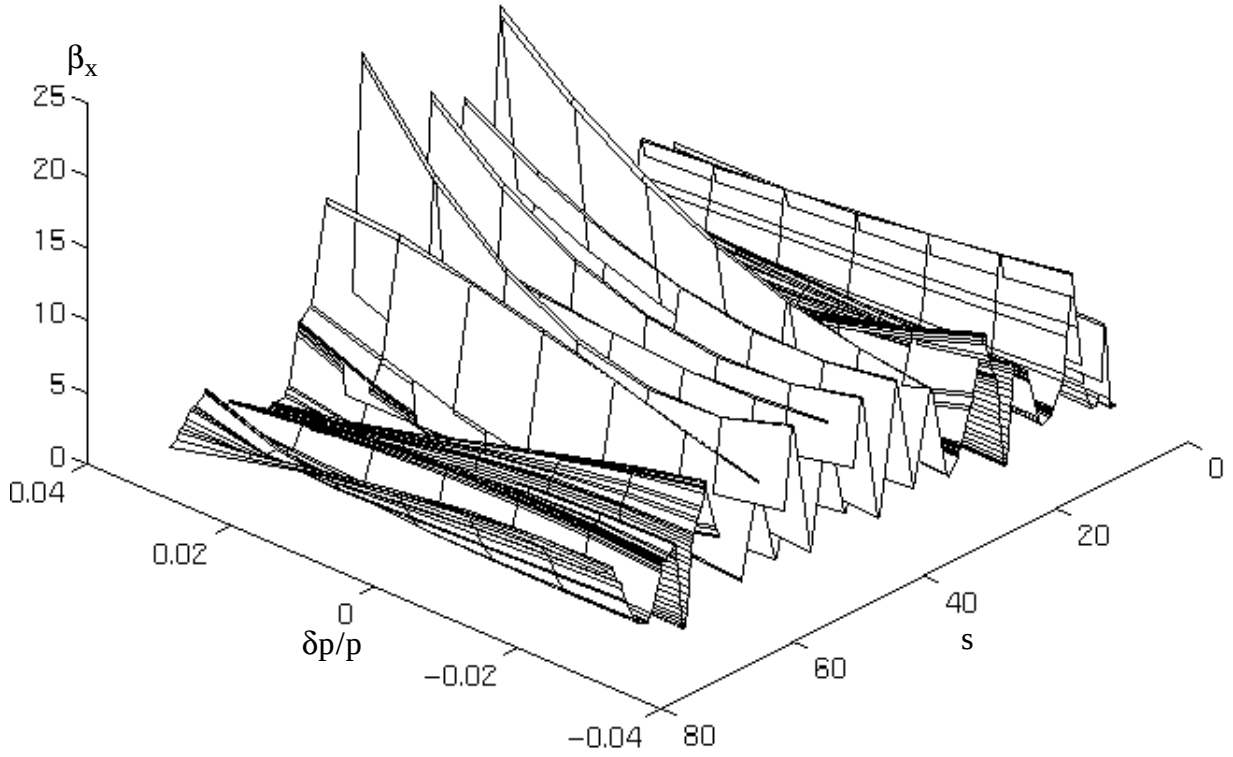

Figure 9a: Horizontal beam envelopes vs. (s, δp/p) from wiggler to reinjection point.

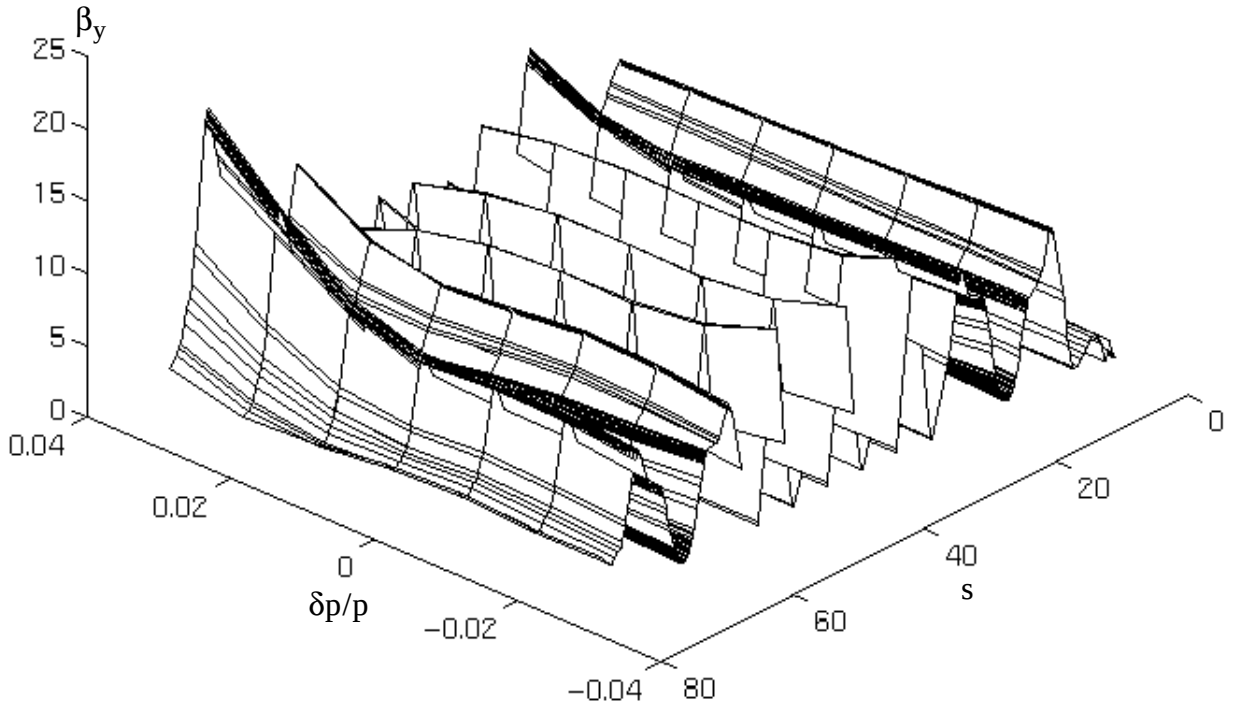

Figure 9b: Vertical beam envelopes vs. (s, δp/p) from wiggler to reinjection point.

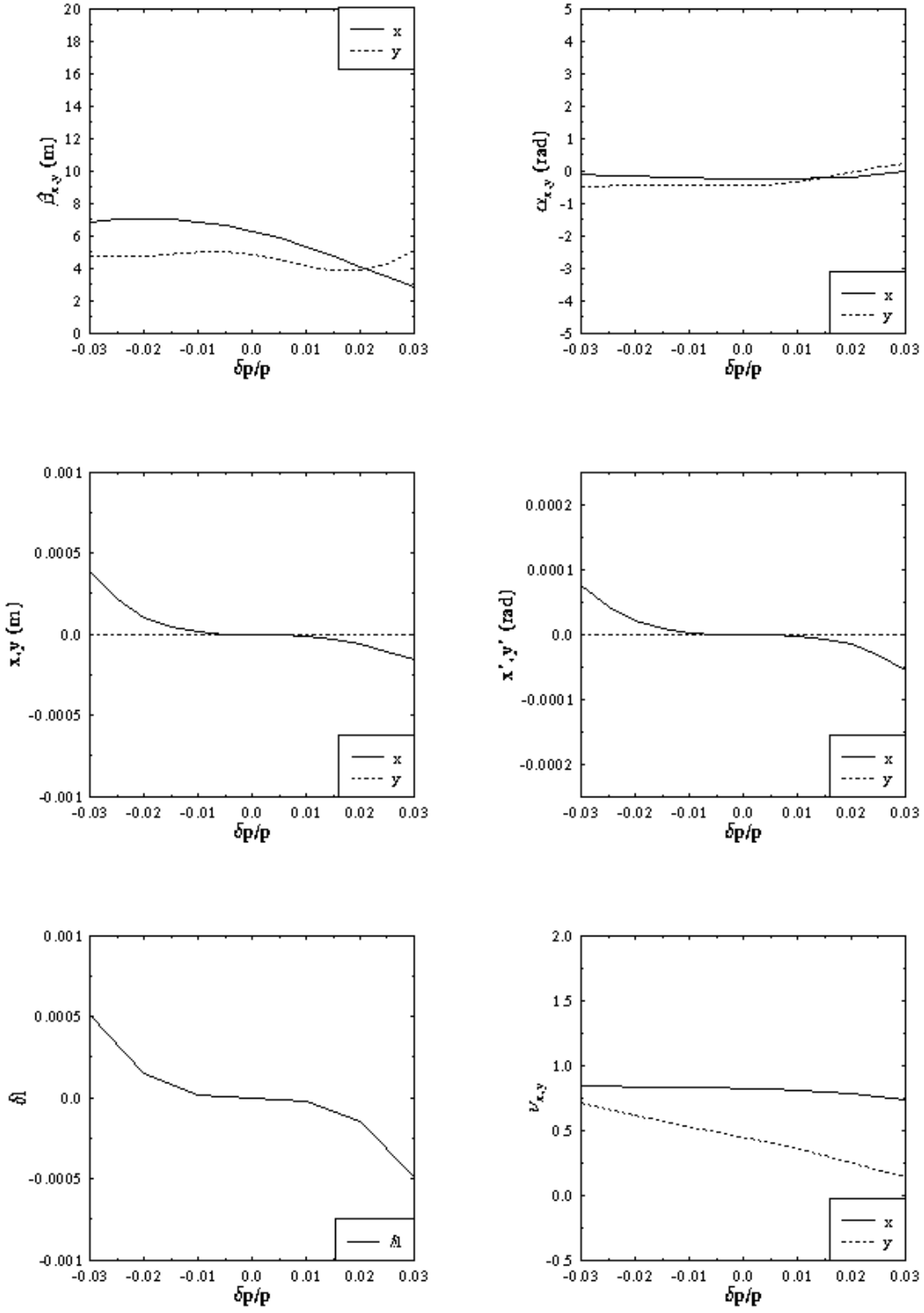

Figure 8b: Beam properties as a function of momentum at the reinjection point after transport from the wiggler.

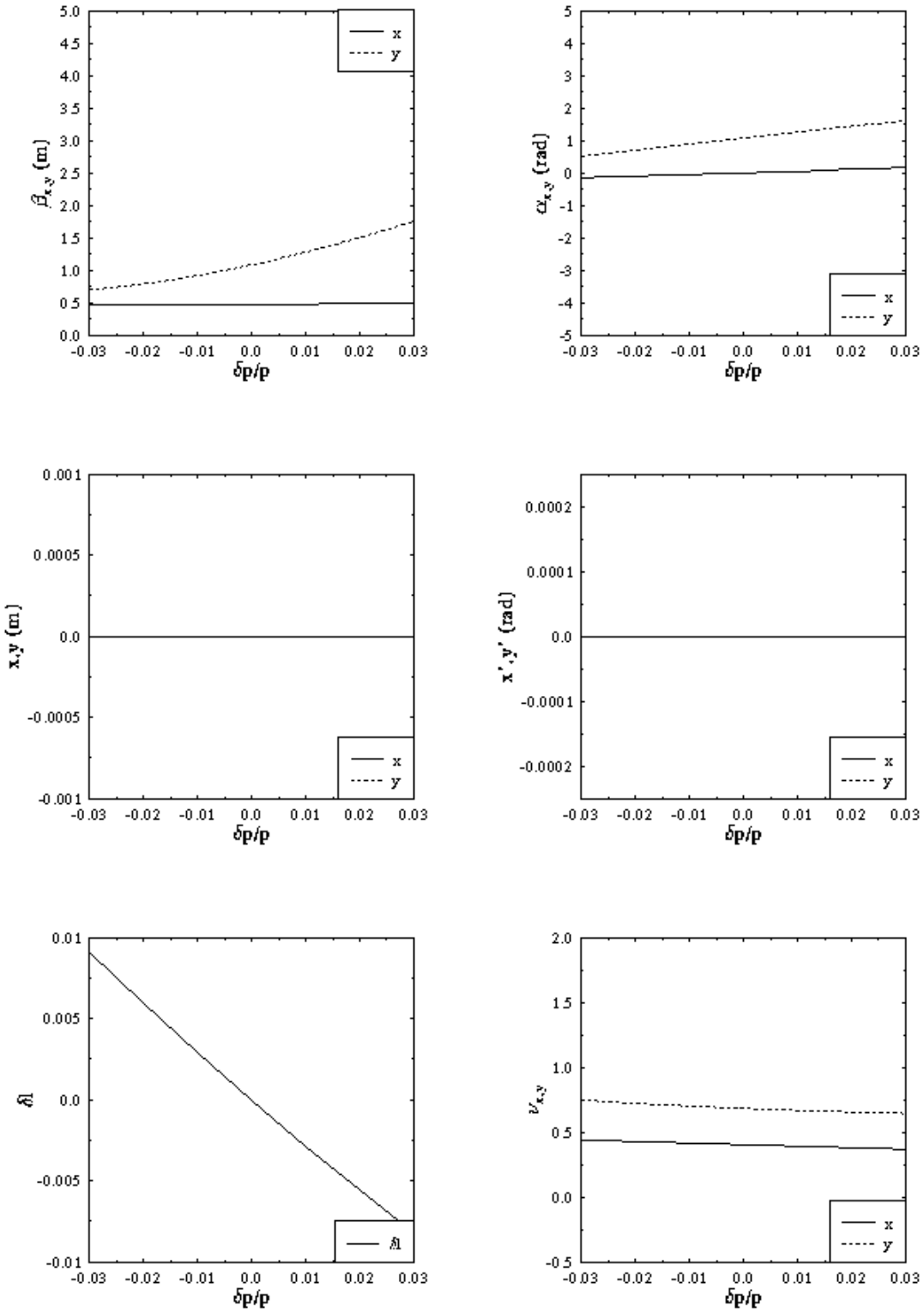

Figure 8a: Beam properties at the wiggler as a function of momentum after transport from the end of the cryomodule.

2B: Matrix from Wiggler to Reinjection Point

FIRST ORDER MATRIX

```
    -.2689779E+01  -.1097294E+01  -.9471558E-17  -.4807566E-15   .0000000E+00  -.7508495E-14
     .3567845E+00  -.2262278E+00   .6730971E-16  -.1100141E-15   .0000000E+00  -.7771561E-15
     .7619918E-15  -.1301877E-15  -.2426310E+01   .2094700E+01   .0000000E+00  -.8893334E-15
     .2291969E-15   .4675888E-17  -.4966376E+00   .1661247E-01   .0000000E+00   .5679691E-16
     .2220446E-14   .1623701E-14  -.5794834E-15   .1337465E-15   .1000000E+01   .3576222E-04
     .0000000E+00   .0000000E+00   .0000000E+00   .0000000E+00   .0000000E+00   .1000000E+01
```

SECOND ORDER TERMS

```
    -.4362665E+01  -.1839295E+02   .9490115E-14  -.1593191E-13   .0000000E+00   .3799300E+01
                    .1457417E+01   .1217777E-14  -.1909904E-14   .0000000E+00   .1550066E+02
                                  -.3909830E+02   .9890374E+02   .0000000E+00  -.4410017E-13
                                                 -.4885143E+02   .0000000E+00   .3798443E-13
                                                                 .0000000E+00   .0000000E+00
                                                                                .8461303E-13
    -.2964432E+01   .7549043E+00   .4234867E-16  -.2761311E-14   .0000000E+00  -.1006283E+01
                    .7341461E+00   .1236539E-15  -.6732530E-15   .0000000E+00  -.2786136E+01
                                   .9814403E+00   .2333266E+01   .0000000E+00  -.3340462E-14
                                                 -.6130882E+01   .0000000E+00   .1970844E-14
                                                                 .0000000E+00   .0000000E+00
                                                                                .3409772E-13
     .1488164E-13   .9629048E-15  -.5347053E+02   .7754817E+02   .0000000E+00  -.4249429E-13
                    .3872524E-15   .6511953E+01   .2051792E+02   .0000000E+00  -.4677435E-14
                                   .2150957E-14   .3752441E-14   .0000000E+00   .9702218E+02
                                                  .5526743E-14   .0000000E+00   .8468888E+01
                                                                 .0000000E+00   .0000000E+00
                                                                                -.1844378E-13
     .4556210E-14  -.1351859E-14  -.2026482E+02   .3300228E+02   .0000000E+00  -.1303865E-14
                    .2686452E-15   .9512654E+01  -.3968169E+01   .0000000E+00  -.4358644E-16
                                  -.9146263E-15   .3558560E-14   .0000000E+00  -.2712323E+02
                                                 -.1024076E-14   .0000000E+00   .2581400E+02
                                                                 .0000000E+00   .0000000E+00
                                                                                -.2725325E-14
     .1957381E+00   .1572198E+01  -.3980436E-13   .3293829E-13   .0000000E+00  -.2676693E-12
                    .3406064E+01   .5586174E-14   .7863581E-15   .0000000E+00  -.7419198E-14
                                   .5759502E+02  -.5945847E+02   .0000000E+00  -.2442332E-13
                                                  .2697841E+02   .0000000E+00   .1288700E-13
                                                                 .0000000E+00   .0000000E+00
                                                                                -.4981317E-04
```

Table 2: Second Order Transport Matrices From Cryomodule to Wiggler and From Wiggler to Reinjection Point for 6 September 1996 Optics

2A: Matrix from Cryomodule to Wiggler

FIRST ORDER MATRIX

-.2823664E+00	.1054076E+01	.2700497E-16	.3017598E-15	.0000000E+00	.1765315E-15
-.8727343E-01	-.3215705E+01	-.9485533E-16	-.3654299E-15	.0000000E+00	-.1999231E-15
-.7679677E-16	.2301115E-16	.1806997E-01	-.2555057E+01	.0000000E+00	.1426471E-17
-.5846343E-17	-.2424655E-15	.3808287E+00	.1492029E+01	.0000000E+00	.5749202E-16
.9367507E-16	.0000000E+00	.4956382E-18	-.1490237E-15	.1000000E+01	-.2887870E+00
.0000000E+00	.0000000E+00	.0000000E+00	.0000000E+00	.0000000E+00	.1000000E+01

SECOND ORDER TERMS

.3884790E-01	.1758808E+00	.7684843E-17	.8417472E-16	.0000000E+00	.2087488E+00
	.3335033E+00	.1006577E-15	.2963711E-15	.0000000E+00	.1207632E+02
		-.2373660E+00	-.1256508E+01	.0000000E+00	.4178625E-15
			-.1113473E+01	.0000000E+00	.1679100E-14
				.0000000E+00	.0000000E+00
					.8798737E-15
-.7635999E-01	-.2603662E+00	-.6451130E-16	-.1779708E-15	.0000000E+00	-.1462277E+01
	-.4124484E+00	-.2859672E-15	-.7710339E-15	.0000000E+00	.6813905E+01
		.3792998E+00	.1546748E+01	.0000000E+00	.3128125E-15
			.1083147E+01	.0000000E+00	.2163590E-14
				.0000000E+00	.0000000E+00
					.1027055E-14
-.4301353E-16	-.2724560E-15	.6627367E+00	.1410127E+01	.0000000E+00	.3727683E-15
	-.5728544E-15	.1899189E+01	.6247876E+01	.0000000E+00	.1767789E-14
		.3942586E-16	.2185956E-15	.0000000E+00	-.4348889E+01
			.4391334E-15	.0000000E+00	-.9419145E+01
				.0000000E+00	.0000000E+00
					-.3543600E-15
.1161929E-17	-.8042921E-17	-.1732383E+00	-.5075509E+00	.0000000E+00	-.3061023E-15
	.1796110E-16	-.1655391E+00	-.1732803E+01	.0000000E+00	-.5678535E-15
		.1904861E-16	.6510333E-16	.0000000E+00	.1170651E+01
			.6717520E-16	.0000000E+00	-.4952694E+01
				.0000000E+00	.0000000E+00
					.2090184E-15
.2278796E+00	-.9620686E+00	-.1312742E-15	-.6867609E-16	.0000000E+00	-.1394595E-15
	.2131334E+02	.6642987E-15	.5293461E-14	.0000000E+00	.3128179E-14
		.8420544E+00	.2524418E+01	.0000000E+00	.2727437E-16
			.1144583E+02	.0000000E+00	-.8409445E-15
				.0000000E+00	.0000000E+00
					.4599486E+00

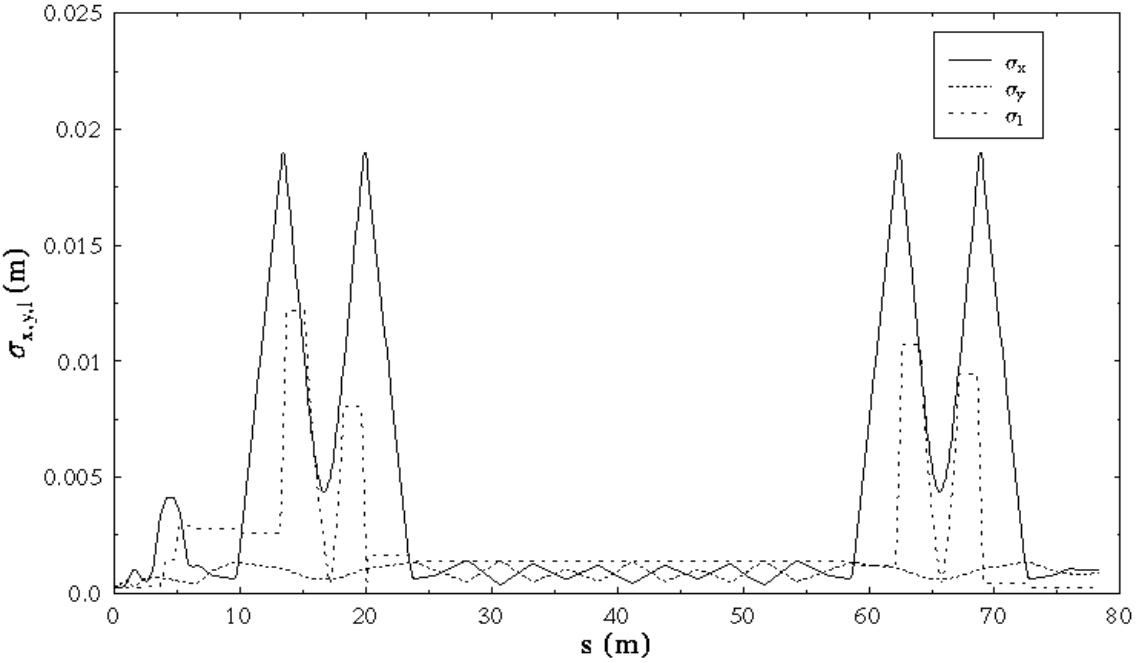

Figure 7: RMS beam spot sizes from wiggler center to linac reinjection point for beam with nominal (13 mm-mrad normalized) emittance, 0.25 mm initial bunch length, and 1% rms momentum spread. Tuning of 6 September 1996 is used.

High-Order Optics Design; Aberration Analysis. We have explored the nonlinear behavior of the machine using the DIMAD "detailed chromatic analysis", "line geometric aberrations" and "tracking" operations. These studies indicate that the baseline design meets all requirements stated above.

Momentum Scans:

Momentum scans of transport system behavior from linac to wiggler and from wiggler to linac indicate performance is adequate. Figures 8-10 show results of momentum scans of beam properties propagated through various portions of the transport system. Figure 8a presents beam properties at the wiggler as a function of momentum after transport from the end of the cryomodule. It demonstrates the beam remains well matched to the wiggler over the full 2% momentum spread of the incident beam. Figure 8b presents beam properties as a function of momentum at the reinjection point after transport from the wiggler. It shows that the full 5% momentum spread of the energy recovered beam remains well behaved at the reinjection point. Figure 9 illustrates the beam envelopes (9a the horizontal and 9b the vertical) as a function of momentum offset throughout the energy recovery transport, from wiggler to reinjection point. Figure 10 shows the horizontal central orbit (the "dispersed offset") through the system at several momentum offsets. Figures 9 and 10 together demonstrate that the full 5% momentum spread of the beam remains well-confined during the energy recovery transport.

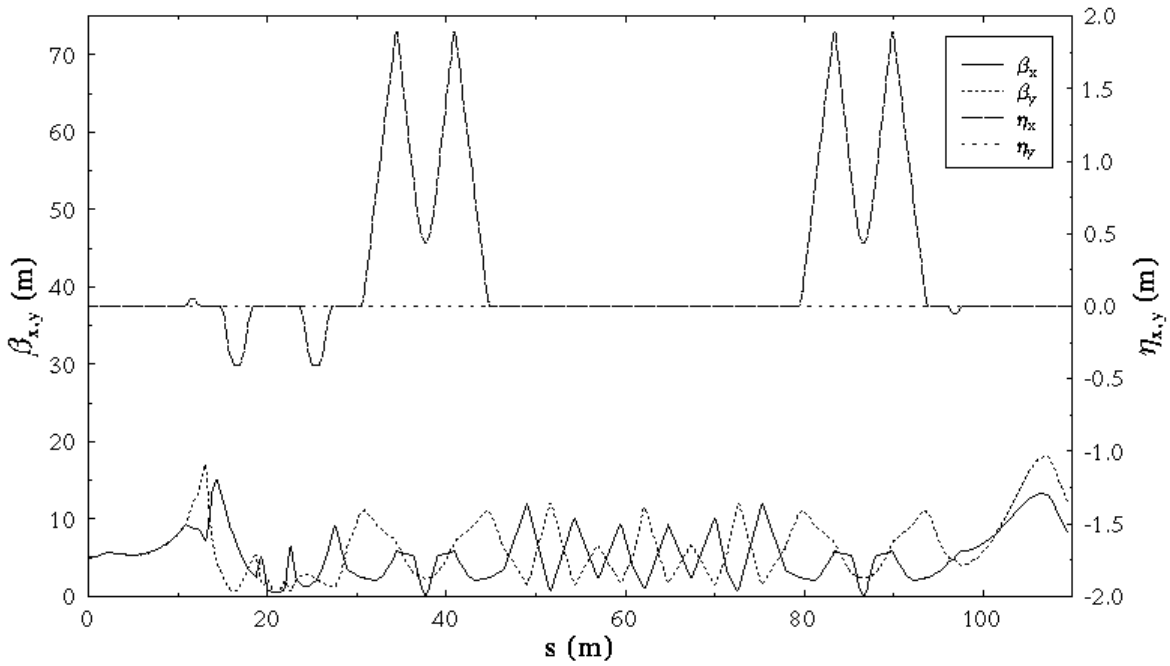

Figure 6: Beam envelopes and dispersions through IR FEL driver (from injection point to dump point) for a study tuning of 6 September 1996, in which the backleg quads are trimmed to accommodate “averaging” of interface quads between the straights and the loops.

Given the above beam envelope functions, we anticipate that the beam will be well confined throughout the acceleration/energy recovery cycle. This is verified by Figure 7, which presents RMS beam spot sizes from wiggler center to reinjection for nominal normalized emittances of 13 mm-mrad (0.16 mm-mrad geometric emittances at 42 MeV), an rms bunch length of 0.25 mm, and 1.0% rms momentum spread. The following observations should be made.

- A well-steered (~1 mm remnant orbit) 6σ beam will be well-contained (*i.e.*, will propagate with a full 1 cm beam stay clear in all transverse directions) in a 5 cm diameter pipe through the straight portion of the machine;
- Larger beam pipe is required for the high dispersion arc, where a rectangular beam pipe of ~20 cm horizontal and 5 cm vertical acceptance is used.
- We note that bunch dimensions in the arcs are different than those assumed in initial CSR estimates, which assumed a short, transversely small bunch. A more accurate picture is being used in estimates that are presently in progress [13].

Other requirements constrain the second order transport matrices from linac to wiggler and from wiggler to linac. These are presented in Table 2. The matrix elements are all of modest magnitude, indicating adequate control of the linear optics and the second order chromatic and geometric aberrations.

Table 1: Beam Optics Requirements Through IR FEL Driver

Location	Constraint	Comment
Transport Through Arc	E=42 MeV $\eta_x=\eta_y=0$; $\eta_x'=\eta_y'=0$ at reinjection, $\beta_{max}<$ 25 m, $\eta_{max}<$ 2 m throughout $\varepsilon_N<$13 mm-mrad $\sigma_{\delta p/p}\sim$1.0%, 5% full width $\lvert M_{56}^{\text{wiggler to module}}\rvert<$0.25 m $\lvert T_{566}\rvert$ nominally zero, tunable over $\sim\lvert T_{566}\rvert<$3 m $T_{166}=T_{266}=0$ $\lvert T_{ij6}\rvert<$100 (m, rad, or 1/m) $(\Delta\beta/\beta, \Delta\alpha)<$ 1 at cryomodule over $\lvert\delta p/p\rvert<$3% $\lvert\Delta\varepsilon/\varepsilon\rvert_{\text{geometric}}<$0.5 over 10 $\varepsilon_{\text{geometric}}$ on $\lvert\delta p/p\rvert<$3%	beam loss, error sensitivity, aberration control bunch compression during energy recovery bunch shaping during compression in energy recovery spot size control at reinjection chromatic aberrations, spot size control, esp. with misteering spot size control at reinjection over full momentum spread geometric aberration control, phase space distortion
Re-injection Point	E=42MeV $\beta_{x,y}\sim$ 5 m, $\alpha_{x,y}\sim 0$ $\eta_x=\eta_y=0$; $\eta_x'=\eta_y'=0$	
Extraction Point	E=10 MeV $\beta_{x,y}\sim$ 10 m, $0<\alpha_{x,y}<1$ $\eta_x=\eta_y=0$; $\eta_x'=\eta_y'=0$ $\beta_{max}<$ 25 m throughout	“full” energy recovery beam loss

IV. System Performance

The system performance meets the requirements stated above.

Low-Order Optics Design. Beam envelope functions and dispersions propagated from the injection point to the energy recovery dump satisfy the peak value requirement and suggest that error sensitivities, aberrations, and loss rates should be well controlled. Design beam envelopes and dispersion are presented in Figure 6.

Table 1: Beam Optics Requirements Through IR FEL Driver

Location	Constraint	Comment
Injection Point	E=10 MeV β_x ~ 5 m, α_x ~ 0 β_y ~ 5 m, α_y ~ 0 $\eta_x=\eta_y=0$; $\eta_x'=\eta_y'=0$ ε_N<13 mm-mrad $\sigma_{\delta p/p}$<0.5% δl<0.6 mm	zero space charge conditions
Transport to Wiggler	E=42 MeV β_x = 0.472 m, α_x = 0 β_y = 0.5 m, α_y = 0 $\eta_x=\eta_y=0$; $\eta_x'=\eta_y'=0$ ε_N<13 mm-mrad $\sigma_{\delta p/p}$<0.5% σ_l(bunch)<0.3 mm $\lvert M_{56}^{\text{module to wiggler}}\rvert$<0.3 m $\lvert T_{566}\rvert$<0.5 m $T_{166}=T_{266}=0$ $\lvert T_{ij6}\rvert$<25 (m, rad, or 1/m) $(\Delta\beta/\beta, \Delta\alpha)$< 0.2 at wiggler over $\lvert\delta p/p\rvert$<1% β_{max}< 25 m throughout $\lvert\Delta\varepsilon/\varepsilon\rvert_{\text{geometric}}$<0.2 over 10 $\varepsilon_{\text{geometric}}$ on $\lvert\delta p/p\rvert$<1%	matched envelope values at center of wiggler length after bunch compression set by RF stability with bunch compression (0.2 m ideal, [CEBAF-TN-95-015] but chicane geometry too congested mechanically at this value) bunch lengthening (2.5 m ideal for M_{56} of 0.2 m, (see TN) but cannot achieve in chicane geometry, must “pre-stress” injected beam and limit aberration in after-cryomodule transport) spot size control at wiggler chromatic aberrations, spot size control, esp. with missteering spot size control at wiggler over full momentum spread beam loss, error sensitivity, aberration control geometric aberration control/ phase space distortion

Other features:
Design characteristics not noted above or warranting greater emphasis are as follows.

- The system uses no external focussing in the linac.
- Adequate beam confinement is provided by the choice of injection condition, linac rf focussing, the focussing effects of the arcs proper, and the matching telescopes.
- Space is available for diagnostic and correction elements; preliminary assignments have been made [11].
- Typical minimum element to element distances exceed ~0.3 m.
- The diameter (linac axis to backleg axis distance) of the system is 5.75 m, set by varying the reverse bend angles (the sector dipoles) while fitting other optical constraints
- the footprint length is ~50 m.
- radii of the major bends are set at 1 m for CSR control purposes.
- As noted above, the M_{56} and path length of the arc can be varied while maintaining achromaticity by appropriately imposed trim quad settings.
- The beam path length is 490.5 RF wavelengths, from injection point to reinjection point.
- Dipole end-field effects are included in all optics computations. For all dipole definitions in DIMAD input decks, a half gap of g=0.0254 m (1 inch) was imposed, and a field rolloff integral K=0.45 was imposed after discussions with L. Harwood. The principle effect of this is to suppress vertical focussing; details are given in a CEBAF Technical Note on error analysis for this machine [12].

A plot of the machine geometry (for the 25 June 1996 implementation of the design) is given in Figure 5. Table 1 presents beam optics requirements through the IR FEL driver.

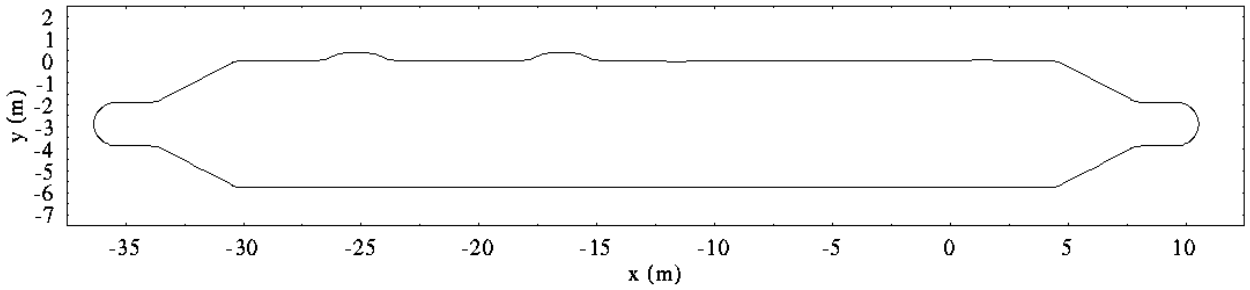

Figure 5: Geometry of IR FEL Driver (25 June 1996 “as built” design file).

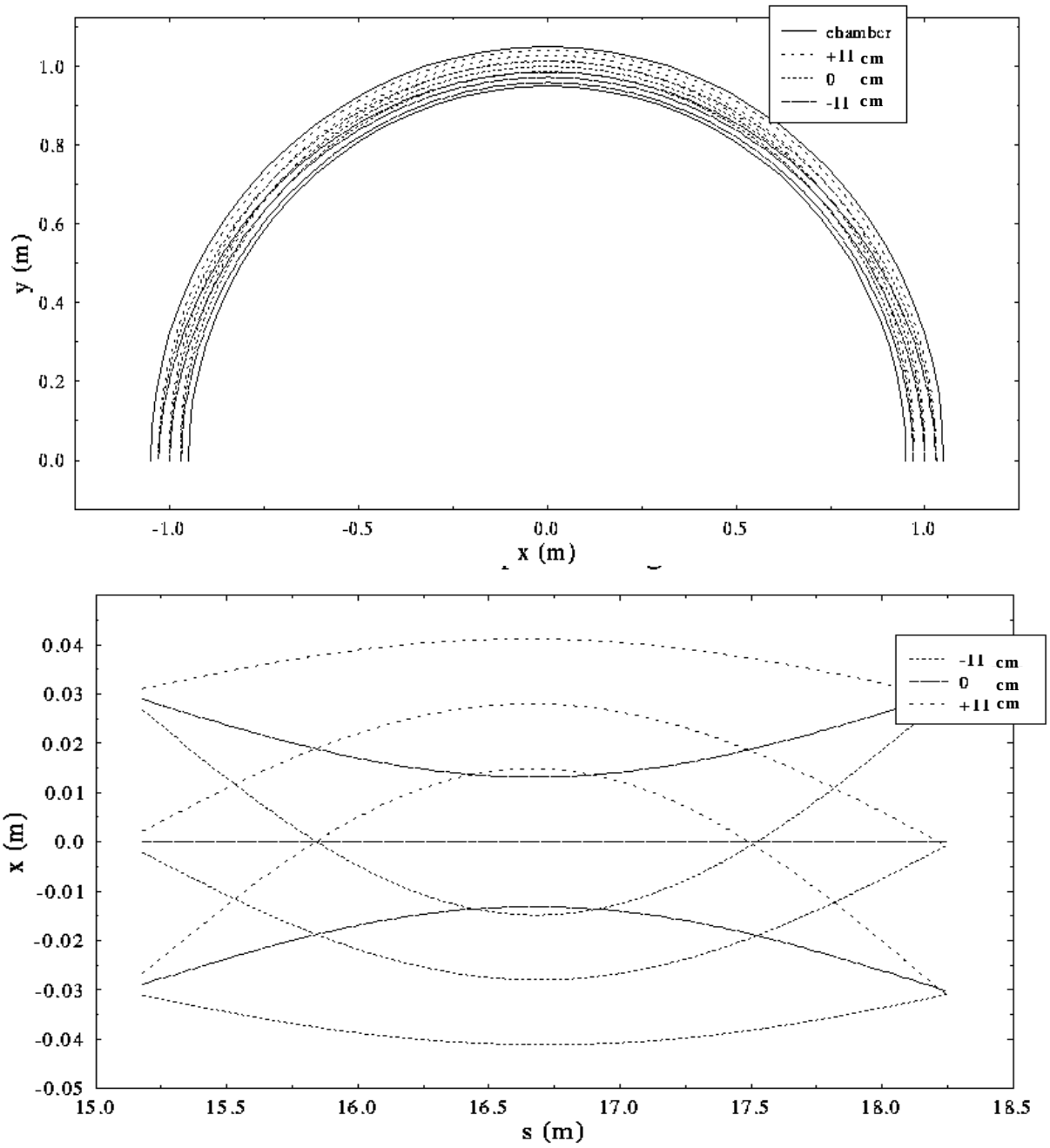

Figure 4: Beam orbits and envelopes in π-bends over full RF period phase variation. Top graphic shows beam size and location for three path length settings; lower graphic illustrates design horizontal beam size through π-bend for the same three settings.

Path Length/Momentum Compaction Control:
The nominal pathlength from injection point to reinjection point (one full circuit of the driver) is 490.5 rf wavelengths. Path length adjustment can be achieved by systematically steering the beam before and after the 180^o dipoles [10]; consideration of the transfer matrix for the "π-bend" shows that systematic steering upstream and downstream of the pole faces of both dipoles by 1 mrad leads to 4 mm path length change with only a 1 mm transverse orbit shift within the dipoles. Figure 4 illustrates the nominal beam size and horizontal position in either π-bend while varying the RF phase through a full period. Ganged horizontal steerers will be provided for this purpose.

Each arc has eight trim quadrupoles (nominally in two families) used to vary M_{56} and/or correct dispersion errors. Use of these trims allows variation of return arc M_{56} over a range of ± 0.25 m with little impact on the properties of the energy recovered beam.

Tunability/Operability:
The design provides no explicit phase advance control to modify beam breakup thresholds. This not only reduces parts count and operational complexity, but also reduces betatron mismatch and chromatic aberrations driven by forcing the phase advance to particular (and usually artificially high) values. It does, however, lead to some lack of operational flexibility. We are therefore concerned with sensitivity to possible changes in focussing (particularly due to injection/extraction chicanes, dipole ends, quadrupole excitation errors, *etc.*) and, as a consequence, must take special care in providing specifications for beam line elements. In addition, much of the chromatic correction is done either in hardware or by optimizing the choice of hardware parameters. Particular effort must therefore be made to accurately predict the chromatic behavior of the system. Details of such computations will be given in the following discussion of system performance.

One can in principle globally modify the recirculator optics using various quadrupole degrees of freedom. The quadrupole singlets at the beginning and end of each recirculation loop provide some capacity for arc dipole end field compensation and phase advance control. An extra degree of freedom is also available in each quadrupole triplet of the two matching telescopes (for a total of four available "knobs"); these provide opportunity for chicane dipole end field compensation and further phase advance control. The nominally uniform FODO backleg quad excitations may be utilized to perform rematches, give phase advance control, modify aberrations or possible to provide CSR suppression.

additional degrees of freedom in beam envelope control through the arc and to or from the matching telescopes.
- The quad singlets are set to minimize vertical beam envelope through arc and to control beam envelopes through the cryomodule module during energy recovery. They can, in principle, also be used to provide phase advance control so as to modify BBU thresholds, should this prove necessary.
- The use of a six quad match from the wiggler into the arc minimizes beam envelope function mismatch and aberrations.
- The backleg of 6 90^o FODO cells provides a 3/2 wavelength image from arc to arc for aberration suppression; the 90^o cells self-correct chromatic aberrations.

The constraints of 1) nominal isochronicity (from wiggler to reinjection point), 2) achromaticity, 3) machine diameter (5.75 m), 4) horizontal tune of 5/4, and 5) vertical transport matrix of M=-I were met for fixed arc dipole bend radius of 1 m by 1) enforcing reflective symmetry about the loop center (achromaticity then reduces to a single constraint), 2) independently varying the edge angles of the 2 families of reverse bends slightly from 1/4 the bend angle, (2 degrees of freedom), 3) independently varying the drift lengths between a. the 2 families of reverse bends and b. the π-bend and reverse bends (2 degrees of freedom) and 4) varying the excitation of the quadrupole singlets at the beginning and end of the loops. Use of a DIMAD “least squares fit” then immediately uses the five degrees of freedom to fit the beam transport constraints; iterating as the angle of the reverse bends is varied allows us to fix the diameter to the desired rational value.

Variation of the quad/reverse bend spacing allows optimization of chromatic aberrations and control over the betatron acceptance of the loop - a judicious choice of drift gives a “nice matched beta”.

Beamline Performance:
The beam envelopes/matrix elements are modest in magnitude, thereby reducing beam size, error sensitivity, and coupling to aberrations. Overall phase advance from injection point to extraction point falls near 5.75 wavelengths horizontally and 4.75 wavelengths vertically.

Chromatic Correction:
Eight sextupoles in two families are provided for aberration control. The required momentum aperture and dispersive orbit control have been achieved with good overall chromatic and geometric aberration sensitivity by simply using these sextupoles to correct T_{166}, T_{266}, and T_{566}. Much of the chromatic aberration control was achieved through optimization of hardware parameters (bend angles, pole face rotations, element separations) to reduce focal aberrations, spurious dispersions, and sensitivity to injection errors. This presumes detailed knowledge of the magnetic properties of elements and assumes “on-line” control or tuning unnecessary. This drives particular concerns with system tunability and with the model used for dipole end fields. Some of these issues are discussed in more detail elsewhere [9].

with $|M_{56}| \leq 0.25$ m. The system uses two five-dipole achromatic, quasi-isochronous 180^o arcs connected by 6 periods of 90^o FODO quadrupole transport (the tuning is mod 1/2 wavelength for aberration suppression).

The system concept is identical to the presentation of Figure 1. We now discuss each sequential sub-module of the transport.

Linac:
The single 30 MeV cryomodule is preceded and followed by 1 m utility drift spaces and injection/extraction chicanes. RF focussing assists in minimizing beam envelopes through acceleration/energy recovery

Injection/Extraction:
The design incorporates the Liu/Neuffer injection line geometry proposed for the CEBAF UV FEL demonstration project [7]. This system employs sector dipoles to provide both bending and radial focussing; the injected or extracted beam is bent through 20^o at a 0.60 m bend radius while the reinjected and recirculated beams are put through chicanes consist of 3 dipoles: 2 outboard wedges (one of which is common with the injected/dumped beam) and a longer inboard bend. The outboard wedges bend the recirculated beams at ~5^o, and the inboard bend (with pole face rotations and contours to suppress dispersions through second order) bends through ~10^o. The system is shown in Figure 3.

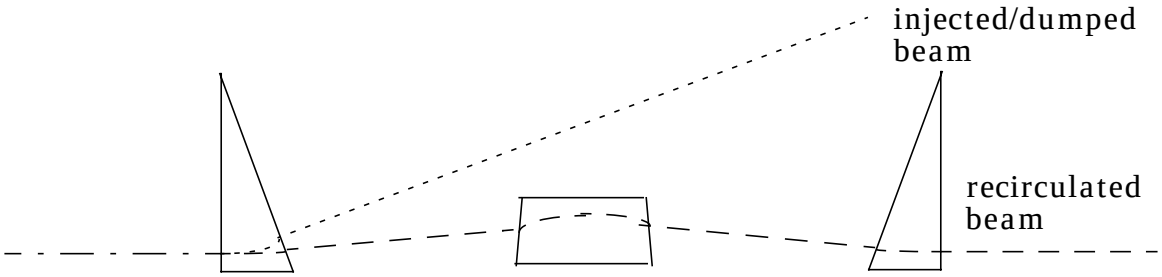

Figure 3: Injection/extraction line configuration using Liu/Neuffer geometry.

Arcs:
The Bates-like arcs [8] are simple beam lines known to provide large acceptance.

- The arcs proper (the “loops”) comprise half-chicanes generated by two families of double-focussing sector dipoles (1 m bend radius, edge angles ~1/4 total bend angle), separated by a single 180^o main dipole of 1 m bend radius. They have betatron tunes of 1.25 in x and 0.5 in y; the vertical transport has M=-I over the full loop.
- The use of double-focussing dipoles minimizes matrix elements/beam envelope functions and provides focussing for the dispersion management necessary for achromaticity and isochronicity.
- Quadrupole singlets are placed upstream and downstream of the arc to provide

A backleg transport consisting of a FODO quadrupole lattice line connects the two recirculation arcs.

We note that the constraints are, in this case, similar to those imposed at MIT:
- Large momentum acceptance is required over the complete recirculation.
- The MIT system is symmetric about the backleg center; this allows passive suppression of some chromatic aberrations. This symmetry is imposed in the IR FEL driver following the match into the first arc, up to the quad just before reinjection.

Design Details

Design Requirements. Specific design requirements are summarized as follows:
- Acceleration from 10 MeV to 42 MeV; transport to FEL at 42 MeV; transport back to the cryomodule at 42 MeV; energy recovery to 10 MeV
- Achromatic transport to the wiggler, with $|M_{56}| < 0.30$ m [6].
- Betatron matching into the wiggler (here assumed to bend vertically and to focus in the nonbending plane only):
  matching to wiggler periodic focussing in non-bend plane;
  matching to upright phase ellipse with $\beta = 0.5$ m at center of wiggler in the bending plane.
- Achromatic transport from wiggler to linac for energy recovery, with variable momentum compaction ($|M_{56}| \leq 0.25$ m).
- Minimal parts count, maximal operational simplicity.
- Large acceptance:
  $\varepsilon_{rms} \sim 0.16$ mm-mrad geometric emittance at 42 MeV
  $\delta p/p \sim \pm 1\%$ from linac to wiggler
  $\delta p/p \sim \pm 2.5\%$ from wiggler to linac
  "acceptance" is here understood to be the region of phase space where beam properties are "good" at the wiggler (*e.g.*, spot size variations ~10% or less) and in which the beam is *well confined* at the linac (*e.g.*, propagated phase space is well defined and regular with spot size variations ~100% or less).
- Good beam envelope control ($\beta^{maximum} < 25$ m), which reduces beam size, error sensitivity, coupling to aberrations, and beam loss.

Design Solution. Acceleration transport comprises
- a 10 MeV injector,
- a single cryomodule supplying 32 MeV acceleration, and
- a six quad telescope matching into wiggler.

Energy-recovery transport comprises
- a second 6-quad match of the wiggler to an energy recovery transport that is
- a Bates recirculator clone, which in this application is modified (through the introduction of trim quadrupoles) to provide variable momentum compaction

determined by Liu [3] to be achievable and to provide adequate beam properties though the acceleration process, even in the presence of space charge.

2. Matching Telescope Issues. A six-quad telescope matching beam from cryomodule to wiggler (with embedded chicane around optical cavity elements) is introduced following the cryomodule. This is illustrated in Figure 2.

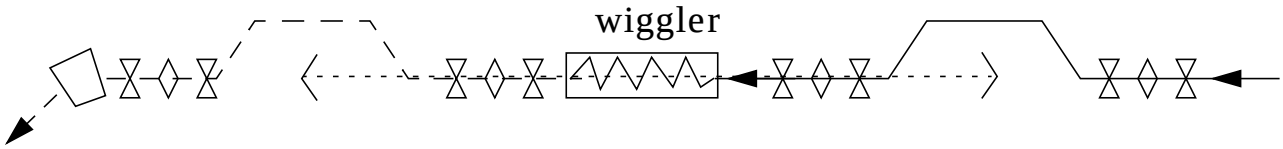

Figure 2: Configuration of matching to/from wiggler using 6-quad telescopes.

- Six quadrupole magnets are use used (despite the fact that the theoretical minimum is 4) to lower peak beam spot sizes, to reduce sensitivity to the focussing effects of dipoles in the embedded chicanes, and to more naturally image the "round" beam from the cryomodule to a "round" beam at the wiggler.
- The second telescope, between wiggler and arc, is needed to image the beam spot into the arc acceptance, keep the spot size small, and limit chromatic aberrations.
- The momentum compaction of the first chicane is accommodated in the Liu scenario [4], in which acceleration is 12.5^{o} off-crest and the chicane time-of-flight variation with momentum is used to give a short bunch at wiggler, even with space charge.

3. Choice of Arc Design. The energy recovery transport must provide adequate beam confinement over a large geometric acceptance and an extremely large momentum range. It should be simple, have minimal parts count, and be rather compact.

Three arc configurations have been considered.

1. The first was an achromatic, isochronous, three-dipole "W" configuration (providing compaction control *via* reverse bending). This was rejected almost immediately because of mechanical congestion, poor chromatic properties, and operational inflexibility (it was, *e.g.*, difficult to change the overall path length and dynamically vary the momentum compaction).
2. The second was a Steffan system with variable momentum compaction (compaction control provided *via* dispersion modulation). This was rejected because of poor chromatic behavior and operational inflexibility (it proved difficult to change the overall path length and was complex to set the sextupoles for proper chromatic correction).
3. The design of choice is based on the MIT-Bates recirculator [5] in which compaction control is obtained *via* both reverse bending and dispersion modulation.

Design Overview

Given the choice of “downstream” FEL, the phase space management requirements detailed above suggest a simple driver concept comprising

- a cryomodule with no external focussing,
- a quadrupole telescope matching to the wiggler
- an achromatic return arc of appropriate betatron acceptance and variable momentum compaction bending back to the cyromodule for energy recovery.

Such a driver is displayed in Figure 1.

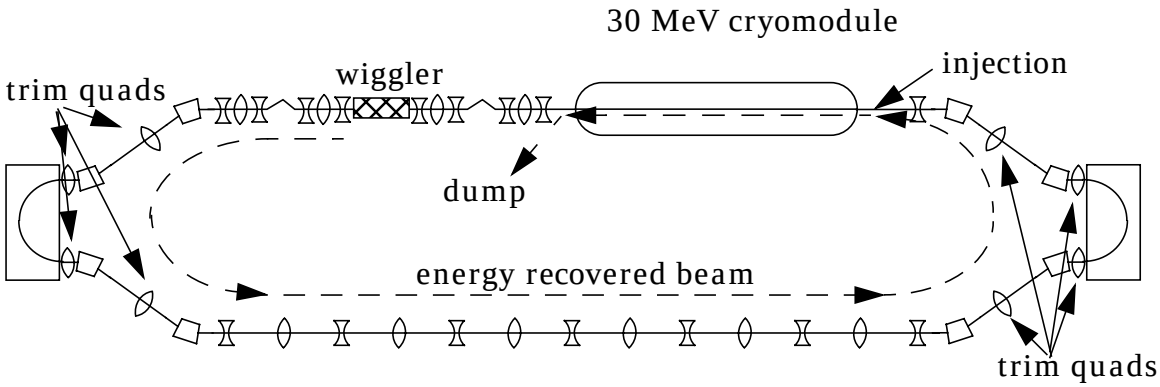

Figure 1: “Downstream wiggler” driver conceptual design.

This concept requires that

- an appropriate combination of rf focussing and injection condition can be achieved for transport through the module without external focussing,
- the dynamic range, acceptance, and chromatic behavior of the telescope matching to the wiggler is adequate to meet the FEL-driven phase space requirements, and
- return arc designs can be developed that meet the required transverse beam confinement and longitudinal phase space management criteria for the large momentum spread ‘spent” beam.

Each of these requirements has been investigated and can be met.

1. Use of RF Focussing. Injection of upright phase ellipses ($\alpha = 0$) with beam envelope function of ~5 m in both transverse planes provides good beam properties through a single cryomodule during off-crest (12.5^{o}) acceleration from 10 MeV to 42 MeV.

- Good beam confinement without external focussing is provided by the RF focussing present in CEBAF cavities at these low energies; details of the beam properties are given in the accompanying discussion of system performance.
- Similarly simple (though numerically different) injection conditions have been

breakup thresholds by adjusting pass-to-pass transfer matrices is desirable but should not introduce undue operational complexity or additional cost.

Space-Charge Management: The design should provide beam confinement from injector through energy recovery even with space charge effects consistent with the 5 mA maximum average current.

Impedance Management: The design should provide beam parameters and mechanical access consistent with the impedance management required for machine performance.

III. System Design

The following fundamental constraint is imposed on all machine configurations for the IR FEL driver:

The cavity pair spacing in CEBAF cryomodules precludes antiparallel acceleration/decceleration of single or multiple beams. The machine under consideration must therefore be a recirculated linac based on a single high-gradient CEBAF module.

The key system design issues are then as follows:

- big phase space
- tight phase space control requirements
- serious beam dynamics questions - space charge, CSR, impedences, BBU
- low energy - “floppy” beam and small, low-field “3-d” magnets
- size/complexity/cost constraints

The design must address these issues and the requirements with sufficient simplicity to meet engineering, cost, and operations constraints, but with adequate flexibility to insure success in achieving 1 kW of light. Three basic concepts are available for the driver layout:

1. *the FEL in the backleg* - an arc transports high quality beam from linac to wiggler; a second arc returns spent beam for energy recovery.
2. *the FEL upstream of the linac* - just prior to energy recovery but after full recirculation
3. *the FEL immediately downstream of the linac* - using the full recirculation only for energy recovery transport of the spent beam.

The latter avoids the CSR issue entirely and therefore (following a 31 January 1996 internal review) has been chosen as baseline concept

energy recovery must give good beam confinement; the design must provide
- betatron acceptance for the (strongly divergent) beam following wiggler,
- the same emittance acceptance as the cryomodule to wiggler transport, and
- acceptance for ±2.5 % momentum offsets to accommodate the 5% relative momentum spread of the spent electron beam. Consequently:
  1. the energy recovery transport will be dispersion suppressed, and
  2. the energy recovery transport will provide variable momentum compaction for beam energy compression during energy recovery. Estimates indicate that M_{56} ~ ±0.25 m provides adequate compression [2].

Low Beam Loss Rates. The system must support FEL operation and energy recovery at beam loss rates allowing safe and stable operation; at anticipated emittances and momentum spreads discussed above and for mechanically reasonable components (maximum apertures not exceeding ~10 to 20 cm) this implies that
- the peak beam envelope functions in the system will not exceed ~25 m, and
- the peak dispersions will not exceed ~2 m.

Mechanical Rationality. The system should be mechanically simple and, if possible, use magnetic components in, or similar to those in, the CEBAF inventory.

Element lengths, strengths, and apertures should be on scales reasonable for a low energy machine (*e.g.*, lengths of a few to several tens of cm, apertures of a few to a few tens of cm, pole tip fields from a few tens to a few hundreds of gauss).

Additionally:
- adequate space should be provided between magnets for mechanical and electrical connections, vacuum components, alignment fixtures, *etc.;* minimum longitudinal spacing ~0.3 m or more.
- allow space for optical cavity components at ±4 m from the wiggler center; give transverse clearances of ~20 cm (8 inches) from optical cavity axis to magnetic components
- space should be allocated for diagnostic and correction system components

Management of Collective Phenomena. As the machine operates with high peak and average currents in a superconducting environment, various collective phenomena must be managed. These force certain constraints on the beam transport system.

CSR Management: Coherent synchrotron radiation (CSR) is an issue of concern; to provide some control of this effect, all bend radii will be at or in excess of 1 m. Beyond this, the design should admit modifications that would allow FEL placement before any bending for energy recovery, so as to avoid the CSR issue altogether.

BBU Management: The design should provide beam breakup thresholds adequate for FEL operation at the 1 kW level. A capacity for operational modification of beam

IR FEL Driver Accelerator Design

D. Douglas

I. Abstract

The design of the “downstream wiggler” IR FEL driver accelerator is described. The following discussion applies to the baseline lattice version of 16 May 1996.

II. Requirements

The top level requirements on the system are as follows:

- beam properties as demanded for IR FEL operation
- accelerator operational demands, including operational simplicity, reliability, and
- accelerator cost considerations.

These translate to lower level requirements on energy, phase space at the wiggler, energy recovery, low beam loss rates, mechanical rationality, and management of several collective effects, including CSR, BBU, space charge, and impedance-driven effects. We now discuss each of these in turn.

Energy. The following requirements are imposed on the beam energy:
- 10 MeV at injection;
- 42 MeV at the wiggler;
- energy recovery to 10 MeV

Phase Space At Wiggler. The following requirements are imposed on the phase space at the wiggler:
- ε_N =13 mm-mrad rms
- $\sigma_{\delta p/p}$ ~ 0.5%; full momentum spread of 2%
- betatron matching to the wiggler
- transport to the wiggler is to be achromatic, provide appropriate bunch length, and have small optical aberrations:
  1. chromatic variation of spot sizes ~10% over the full beam momentum spread,
  2. geometric aberration degradation of the beam spot size will remain at or below ~10% over the full beam momentum spread, and
  3. momentum compaction (M_{56}) of the linac to wiggler transport will be limited to values allowing reasonable RF stability tolerances (typically, less than 30 cm in magnitude [1]).

Energy Recovery. The design must avoid rf power costs/limitations and limit radiation activation by the electron beam following the FEL by energy recovery of the “spent” beam from 42 MeV to 10 MeV. The transport from wiggler to cryomodule for